Transonic Flow Calculations Using Triangular Finite Elements

Richard B. Pelz* and Antony Jameson†
Princeton University, Princeton, New Jersey

This paper describes a technique for finding the numerical solution of the full potential equation for steady transonic flow about airfoils. The exterior, but finite, domain is discretized by breaking it into triangles. Difference equations are formulated using a variational principle and a formula for the derivative in an arbitrary polygon. The iterative schemes include a multigrid-ADI for structured grids and a three-level Jacobi for more arbitrary grids. Results show consistency and compare favorably with codes using quadrilateral elements.

Introduction

SOLUTIONS to the potential flow equation have been shown to give accurate predictions of the aerodynamic characteristics of streamlined bodies at low transonic speeds. Computer codes that solve numerically for the potential flow about wings and airfoils, coupled with a boundary-layer correction algorithm, provide crucial design and analysis tools for efficient shapes in the new generation of commercial aircraft.

For a single airfoil in an external domain, fast and reliable methods exist to generate a grid and to solve the resulting difference equations. Now the task before the computational aerodynamicist is to develop techniques to find the solution over more complicated geometries such as multielement airfoils.

The augmentor airfoil,[1] for example, is an asymmetric airfoil with two aft auxiliary foils originally designed for STOL purposes. It has been shown experimentally to have surprisingly low drag and efficient maneuvering chracteristics at transonic speeds. Whether these characteristics are due to viscous effects or are a property of the inviscid flow is a question that may be answered through analysis of the potential flow about such a configuration.

In obtaining the difference equation, the two best known ways that are suited for handling complex geometries are the finite element and finite volume methods. The mapping function from the computational to the physical domain used to transform the equations in the finite difference method is not needed for the finite volume method because the difference equation is formulated in the physical plane. In finite element theory, the governing differential equation is replaced by a variational principle and solution methods can be applied directly in the physical plane.

The most commonly used element to date has been the quadrilaterial with a bilinear variation of the potential and isoparametric representation. However, the triangular finite element has some interesting advantages. First, the triangle is the simplest two-dimensional geometric figure with area; thus one would think that grid generation around complex geometries might be easier than with quadrilaterals. For example, the discretization of an n-element airfoil and far-field boundary produces an $n+1$ connected domain with a polygonal boundary. It can be proved that both triangle and quadrilateral finite elements can cover this domain exactly, but triangulation might be done in a more efficient manner.

Second, if one restricts the potential to vary linearly between the vertices of a triangle, then the gradient (the velocity) is constant within the triangle. Hence there is no error associated with integration of the variational, since the integrand is a function only of the velocity. The difference equation reduces to a simple formula that can be thought of as a mass flux balance on a secondary polygonal cell around the node. The retarded density/artificial compressibility method is used to modify the difference scheme in order to enforce the entropy condition.

The more complex the geometry, the harder it is to create grids that have structure, i.e., that have each grid line being parameterized with a variable varying in a monotonically increasing fashion. The existing methods (patching, conformal mapping, solving nonlinear elliptic equations, and integral curve methods[4]) all have difficulties in generating efficient curvilinear coordinate systems around n-element airfoils. Inevitably the aspect ratio of some elements becomes large, which leads to inaccuracies.

On the other hand, one can fit a completely unstructured grid of fairly low-aspect-ratio elements about almost any domain. One of the authors is currently developing an algorithm to cover a domain with triangles that have strict bounds on their aspect ratio. The use of an unstructured grid restricts the choice of the iterative scheme. Point schemes are the only alternative, unless one wants to invert directly the full, sparse, but unstructured matrix and use a Newton-type iteration.

Depending on the structure, one of two iterative schemes were used on the triangular grids. A multilevel iterative scheme was constructured based on the Jacobi scheme for unstructured grids. A fast iterative method, multigrid-ADI (alternating direction implicit), was used on the structured grids.

This paper discusses the derivation of the difference scheme on triangles and tries to establish its accuracy and usefulness in computing the transonic flow around airfoils.

Derivation of Difference Equations

In this section the difference equations for triangular elements are derived, some physical implications of the equations are discussed, and the imposition of the boundary conditions is described.

Consider the general problem of writing a difference equation in an arbitrary polygon. In particular, consider estimating df/dx in an arbitrary polygon with N-1 sides, where values of f are given at each of the N nodes. First define the average value

Presented as Paper 83-1922 at the AIAA Sixth Computational Fluid Dynamics Conference, Danvers, Mass., July 13-15, 1983; received Dec. 6, 1983; revision received May 25, 1984.

*Presently, Postdoctoral Associate, Massachusetts Institute of Technology, Cambridge, Mass. Member AIAA.
†Professor. Member AIAA.

of df/dx as the area integral over the polygon,

$$\frac{\overline{\partial f}}{\partial x}=\frac{1}{A}\iint\frac{\partial f}{\partial x}\mathrm{d}x\mathrm{d}y \tag{1}$$

where A is the area of the polygon. Using Green's theorem, the expression becomes

$$\frac{\overline{\partial f}}{\partial x}=\frac{1}{A}\oint f\mathrm{d}y \tag{2}$$

and taking a representative value of f for an edge to be the average of the end-point values, one finds

$$\frac{\overline{\partial f}}{\partial x}\cong\frac{1}{A}\sum_{k=1}^{N}\frac{f_{k+1}+f_k}{2}(y_{k+1}-y_k) \tag{3}$$

The index $N+1$ is 1. The same procedure gives an exact equation for the area,

$$A=\iint\mathrm{d}x\mathrm{d}y=\oint x\mathrm{d}y=\sum_{k=1}^{N}\frac{x_{k+1}+x_k}{2}(y_{k+1}-y_k) \tag{4}$$

Restricting one's attention to triangles, define the velocity potential as the function defined at the nodes; assume further that the potential varies linearly between the nodes. The polygon formula derived above gives exact expressions for the velocities u and v. Since three points determine a plane, the trial function in a triangle is an equation for a plane and the gradient will be constant within the triangle. See Fig. 1a.

This representation of the potential is analogous to the area basis functions of the finite element theory,[5] see Fig. 1b. The trial function is

$$\phi=\phi_1A_1+\phi_2A_2+\phi_3A_3 \tag{5}$$

where

$$A_1=\frac{x(y_3-y_2)+x_2(y-y_3)+x_3(y_2-y)}{x_1(y_3-y_2)+x_2(y_1-y_3)+x_3(y_2-y_1)}$$

$$A_2=\frac{x_1(y_3-y)+x(y_1-y_3)+x_3(y-y_1)}{x_1(y_3-y_2)+x_2(y_1-y_3)+x_3(y_2-y_1)}$$

$$A_3=\frac{x_1(y-y_2)+x_2(y_1-y)+x(y_2-y_1)}{x_1(y_3-y_2)+x_2(y_1-y_3)+x_3(y_2-y_1)} \tag{6}$$

For a difference scheme to be compatible, the potential must be continuous between elements. Compatibility is insured in triangles by the linearity of the potential; no isoparametric representation is needed.

The variational principle for compressible, inviscid, irrotational flow was described by Bateman.[6] Consider the integral

$$I=\iint P(\nabla\phi)\mathrm{d}x\mathrm{d}y \tag{7}$$

where P is given by the isentropic relation

$$P=\frac{1}{\gamma M_\infty^2}\rho^\gamma,\quad \rho=\left[1+\frac{\gamma-1}{2}M_\infty^2(1-\nabla\phi\cdot\nabla\phi)\right]^{1/(\gamma-1)} \tag{8}$$

The solution ϕ of the continuity equation for a compressible, inviscid, irrotational flow is a stationary point of the integral. This can be seen by noting that the Euler-Lagrange equation of I is the continuity equation, since

$$\frac{\partial P}{\partial u}=-\rho u\ \text{ and }\ \frac{\partial P}{\partial v}=-\rho v \tag{9}$$

The integral can be cast as the sum of integrals over the N triangles that make up the domain,

$$I=\sum_{i=1}^{N}\iint P\mathrm{d}x\mathrm{d}y \tag{10}$$

Because of the constant gradient, the pressure is constant in each triangle; thus

$$I=\sum_{i=1}^{N}P_iA_i \tag{11}$$

Taking the first variation one finds that

$$\delta I=\sum_{i=1}^{N}\left[\left(\frac{\partial P}{\partial u}\right)_i\delta u_i+\left(\frac{\partial P}{\partial v}\right)_i\delta v_i\right]A_i \tag{12}$$

from the polygon formula $(\delta u,\delta v)_i$ can be written

$$\begin{aligned}(\delta\nabla\phi)_i&=\left(\frac{\partial\nabla\phi}{\partial\phi_1}\delta\eta_1+\frac{\partial\Delta\phi}{\partial\phi_2}\delta\eta_2\frac{\partial\nabla\phi}{\partial\phi_3}\delta\phi_3\right)_i\\&=\frac{1}{2A_i}[(y_2-y_3)(x_3-x_2)\delta\phi_1\\&\quad+(y_3-y_1)(x_1-x_3)\delta\phi_2+(y_1-y_2)(x_2-x_1)\delta\phi_3]_i\end{aligned} \tag{13}$$

where the subscripts *1*, *2*, and *3* refer to the three vertices of the ith triangle.

Reordering in terms of the points $j=1,2,\ldots,M$, the expression for the first variational becomes

$$\delta I=-\sum_{j=1}^{M}S_j\delta\phi_j \tag{14}$$

where

$$S_j=\frac{1}{2}\sum_{k=1}^{6}\rho_k(u_k\Delta y_k-v_k\Delta x_k) \tag{15}$$

and where j is the index for the center point, k the index of the surrounding six triangles, and Δx and Δy the lengths of the leg opposite the jth node. See Fig. 2.

The discrete Euler-Lagrange equation is

$$S_j=0 \tag{16}$$

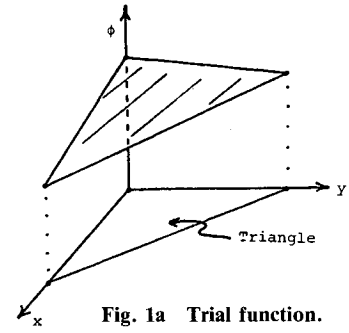

Fig. 1a Trial function.

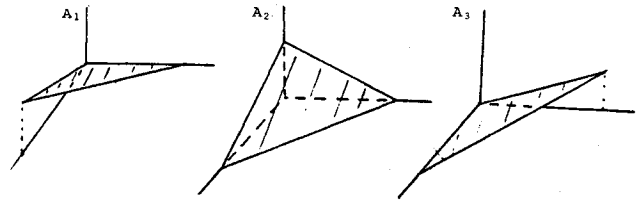

Fig. 1b Basis functions.

at every point j, $j=1,2,\ldots,M$. Physically,

$$\tfrac{1}{2}\rho(u\Delta y - v\Delta x) \tag{17}$$

is a mass flux through some surface in the jth triangle. A representative surface is the dotted one in Fig. 3a, the end points being the midpoints of the two legs extended from the jth node. Since the density and velocity are constant, the surface that extends through the midcell point is equally representative (Fig. 3B). Thus, S approximates a mass flux in a secondary cell formed from the midcell points. Because the secondary mesh is interlocking, the domain is completely covered once (Fig. 4a).

Consider the six-triangle group pictured in Fig. 5a; for Laplace's equation, the flux balance becomes just the discrete Laplacian,

$$S_j = (1/\Delta x^2)(\phi_1 - 2\phi_0 + \phi_4) + (1/\Delta y^2)(\phi_2 - 2\phi_0 + \phi_5) \tag{18}$$

Consider further the group in Fig 5b; the flux balance equation for Laplace's equation is

$$\Delta^2 S_j = (\phi_1 - 2\phi_0 + \phi_4) + (\phi_2 - 2\phi_0 + \phi_5) + (\phi_3 - 2\phi_0 + \phi_6) \tag{19}$$

This equation is logical if one appeals to the mean value theorem for harmonic functions.

The boundary conditions are

$$\phi \to \frac{1}{2\pi}\tan^{-1}\left(\sqrt{1-M^2_\infty}\,\frac{Y}{x}\right) \text{ as } x,y\to\infty \tag{20}$$

in the far field and

$$\frac{\partial\phi}{\partial n} = 0 \tag{21}$$

on the airfoil. The difference equation for points on the airfoil involves only three triangles. The mass flux balance still holds, however, with just the three. See Fig. 4b.

For the solution to be unique, the Kutta condition (that the flow leaves the trailing edge smoothly) must be enforced. A branch cut, across which there is a constant jump in the potential from the airfoil to the outer boundary, is also necessary if a bound vortex is contained in the airfoil. Since there are actually two values of the potential at a point on the cut, there must be two conditions. One is

$$\phi^+ - \phi^- = \Gamma - \text{const along cut} \tag{22}$$

and the other is that the flux balance hold. In the special case of the trailing-edge point, the flux balance from the upper secondary cell will supply the flux into the lower secondary cell and vice versa, thus giving two conditions.

In supercritical flows, nonuniqueness can be caused by expansion shocks, which can appear as a result of ignoring the second law of thermodynamics. A biasing of the difference scheme upstream provides a way to exclude the nonphysical solutions. The addition of the proper upwind bias is accomplished by moving the point of evaluation of the densities slightly upstream. This method of retarding the densities was developed by Eberle[7] and Hafez et al.[8]

The quantity

$$\frac{\partial\rho}{\partial s} = \left(\frac{\partial\rho}{\partial x}u + \frac{\partial\rho}{\partial y}v\right)\Big/ q \tag{23}$$

is evaluated at the nodes if the averaged Mach number is greater than some cutoff number, $M_c \le 1$. Equation (23) is calculated using the polygon formula on the polygon formed by the secondary cell. The density of a triangle is then modified by locating the node that is nearest to the upstream direction from the triangle centroid (node 1 of Fig. 6) and

$$\tilde{\rho} = \rho - \delta\left(\mu\frac{\partial\rho}{\partial s}\right)_1 \tag{24}$$

where δ is the distance between the centroid and node 1 and where

$$\mu_1 = \max(1 - M_c^2/M^2, 0) \tag{25}$$

The modified densities replace the regular densities in the flux balance formula. This procedure makes for a fully rotated scheme; however, it lowers by one the order of accuracy.

Grid Generation

Two types of triangular grids were used to test the difference equations: a structured one produced by placing diagonals on a quadrilateral grid and an unstructured one produced by an algebraic method.

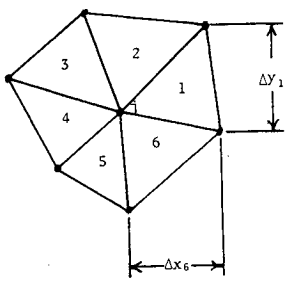

Fig. 2 Difference formula stencil.

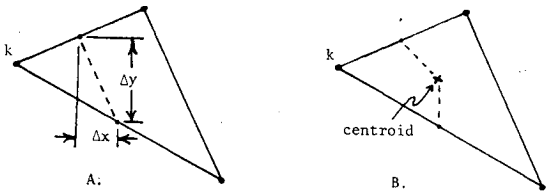

Fig. 3 Flux line and modification.

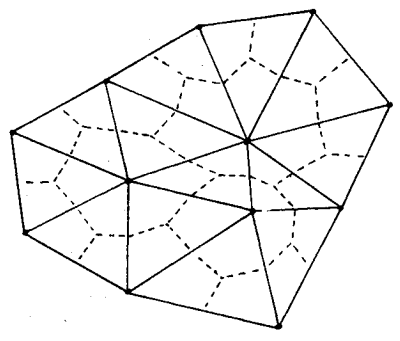

Fig. 4a Secondary cell system.

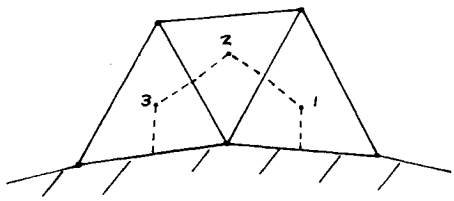

Fig. 4b Three-cell boundary.

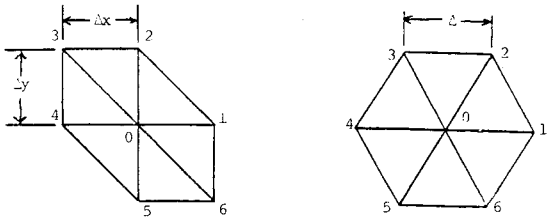

Fig. 5 Examples of simple hexagon systems.

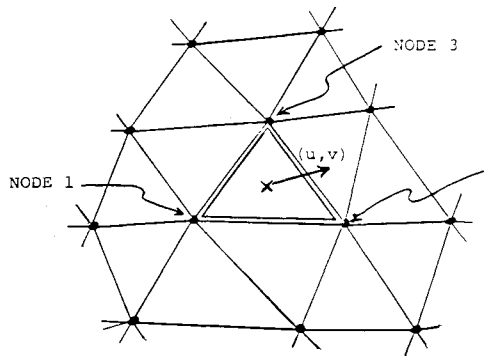

Fig. 6 Upwinding of the density.

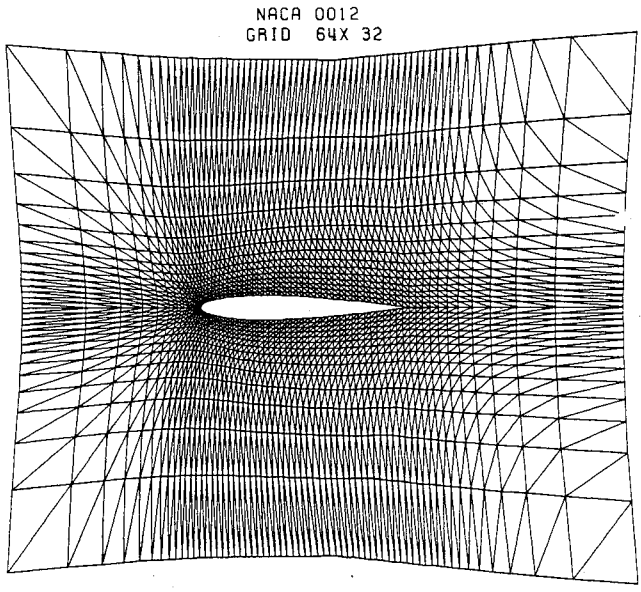

Fig. 7 Triangular grid with structure.

The quadrilateral grid is generated by an airfoil-to-slit transformation, producing an H-type grid. A square root transformation maps the input airfoil and slit computational domain to the upper half planes. The mapped airfoil coordinates are then added to the comptuational plane by a shearing map. The physical plane is generated using a square map on the sheared plane. There is a sparseness of points around the leading edge that is corrected by a nonorthogonal map in the intermediate plane. The resulting grid is shown in Fig. 7; for more details, see Pelz and Steinhoff.[9]

The algebraic algorithm was originally developed by Bank[10] and is still being modified for n-element airfoil grids by one of the authors. Basically, it takes a simply connected domain and searches the boundary to find three adjacent points that satisfy the criterion

$$4\sqrt{3}A/(h_1^2+h_2^2+h_3^2)\geq\beta \tag{26}$$

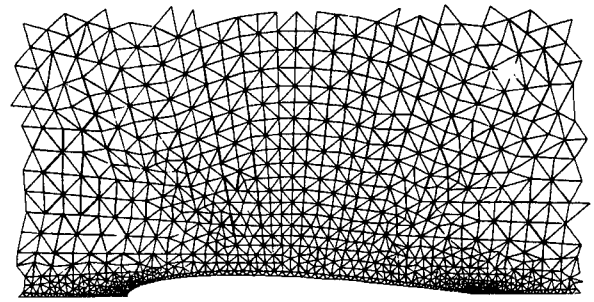

Fig. 8 Unstructured grid around NACA 0012 airfoil (128 points).

where A is the area and h the distances between the points. For high-quality triangles, $\beta=0.5$ gives an aspect ratio of less than 13/4 for isoceles triangles.

If the resulting domain is still a many-sided polygon, it is split into two domains and the searching is done on both domains. This procedure continues until the domain is completely covered. One typical result is shown in Fig. 8. An advantage of the method is that one has control in the placement of the triangles.

Iterative Scheme

On the structured grid, rapid covergence was obtained using a multigrid method adapted for transonic flow problems by Jameson.[11] The linear differential equation

$$L[\phi]=f \tag{27}$$

can be approximated on a grid of mesh size h by

$$L^h[\phi^h]=f^h \tag{28}$$

Letting the initial guess by ϕ_0^h, there exists a correction $\delta\phi^h$ such that

$$L^h[\phi_0^h+\delta\phi^h]=f^h \tag{29}$$

Instead of solving for the correction on the grid of mesh size h, one solves for it on a grid of mesh size $2h$,

$$L^{2h}[\delta\phi^{2h}]=I_h^{2h}\{f^h-L^h[\phi_0^h]\} \tag{30}$$

where I is an operator transferring the values from the h to the $2h$ grid. The fine-grid residual becomes the forcing function for the coarse-grid problem. Using the same procedure, the problem can be cast on the $4h$ grid.

To transfer the correction from the coarse to fine grid, an interpolation operator is defined as

$$\phi_1^h=I_{2h}^h\delta\phi_0^{2h}+\phi_0^h \tag{31}$$

At each step a smoothing operator is used to damp the errors caused by the transfer.

In this way, the signal propagation per iteration is increased to the width of the largest grid and the errors in each frequency band are damped on an appropriate grid. This method is extended to nonlinear problems by using the full approximation scheme of Brandt,[12]

$$L^{2h}[\phi_1^{2h}]=I_h^{2h}\{f^h-L^h[\phi_0^h]\}+L^{2h}[\phi_0^{2h}]$$

$$\phi_1^h=\phi_0^h+I_{2h}^h\{\phi_1^{2h}-\phi_0^{2h}\} \tag{32}$$

The algorithm to damp the high-frequency errors (aliased on coarser grids) at each multigrid step is a generalization of the alternating direction scheme of Peaceman and Rachford.[13]

The left side of the correction-residual equation

$$\alpha N\delta\phi^n = \omega L(\phi^n) \tag{33}$$

is factored in a way approximating L,

$$\alpha N = (\alpha - A\delta_x^2)(\alpha - B\delta_y^2) \tag{34}$$

where

$$A \sim \rho(1-u^2/a^2), \qquad B \sim \rho(1-v^2/a^2)$$

ω is the relaxation parameter, and α a parameter to be chosen.

Since Eq. (34) yields a parabolic equation in psuedotime, the parameter α is replaced by the operator

$$\alpha = \alpha_1 + \alpha_2\delta_x + \alpha_3\delta_y \tag{35}$$

giving a hyperbolic equation necessary in supersonic flow. The choice of α_1, α_2, and α_3 is made to keep the proper domain of dependence.

For unstructured grids where neighboring points can be considered to be independent of each other, a point scheme is necessary. Since successive schemes require updated neighboring nodes, the Jacobi scheme is the only one possible.

Consider the two-step Jacobi scheme,

$$a(\delta\phi^{n+1} - \delta\phi^n) + b\delta\phi^n = \omega L(\phi^{n+1}) \tag{36}$$

where

$$\delta\phi^n = \phi^{n+1} - \phi^n$$

It requires the same order operations to obtain a converged solution at point SOR, which is a considerable gain over the single-step Jacobi.

Consider further a modification of the three-level scheme to supersonic flow by the addition of a streamwise derivative of the correction.[14] To analyze this, the time analogy is used on the quasilinear equation,

$$\alpha\phi_{tt} + \beta\phi_{st} = -(M^2-1)\phi_{ss} + \phi_{nn} \tag{37}$$

Letting

$$T = t - \beta/[2(M^2-1)], \quad S = s, \quad N = n \tag{38}$$

gives

$$\{\alpha - \beta^2/[4(M^2-1)]\}\phi_{TT} = -(M^2-1)\phi_{SS} + \phi_{NN} \tag{39}$$

Requiring S to be the timelike direction restricts

$$\beta > 2\sqrt{\alpha(M^2-1)} \tag{40}$$

The modification is realized on triangles by

$$\alpha(\delta\phi^{n+1} - \delta\phi^n) + \beta\Delta s\frac{\partial(\delta\phi^n)}{\partial s} = \omega L(\phi^{n+1}) \tag{41}$$

The second term on the left can be calculated by the polygon formula for the derivative in the triangle directly upstream of the node in question.

Results

In this section the triangular finite element method is analyzed by examining the numerical solutions of the full potential equation. Examples with both structured and unstructured grid and their associated iterative schemes are included. Solutions are compared with Jameson's FL042 code[3], which uses the finite volume method, quadrilateral elements, and an O-type grid.

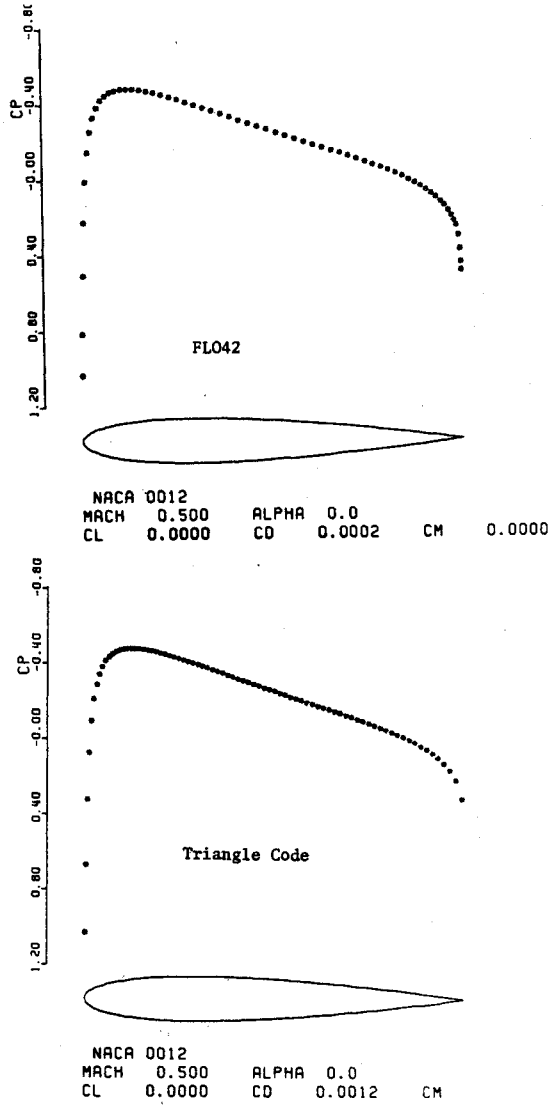

Fig. 9 Pressure distribution for subcritical case: structured grid.

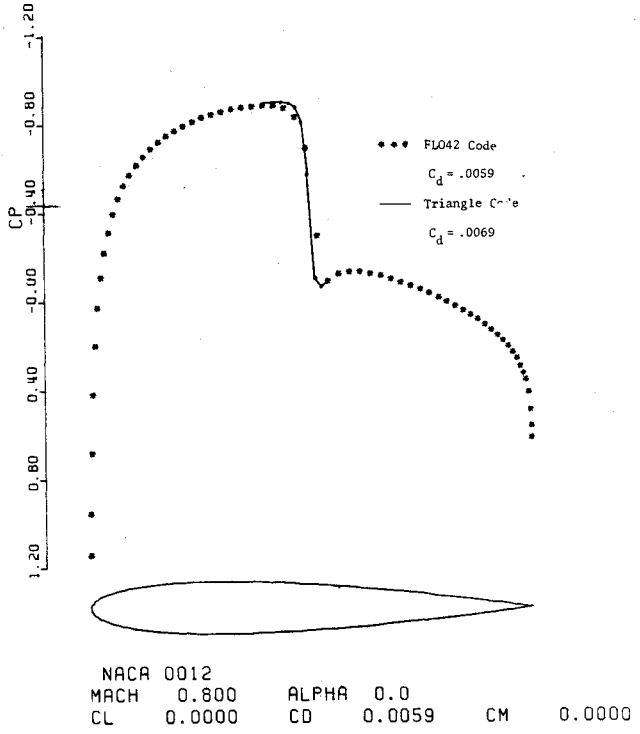

Fig. 10 Pressure distribution for supercritical case: structured grid.

Figure 9 shows the pressure distribution over a NACA 0012 airfoil with a freestream Mach number of 0.5 and a 0 degree angle of attack. The solution using the triangle finite element method was performed on the H-type grid. The grid points for both the triangle and FL042 codes number 128 in the x (circumferential) direction and 32 in the y (radial) direction. A discrepancy between the solutions occurs only at the trailing edge—where the triangle code fails to adequately resolve the stagnation point. This is believed not to be due to the inaccuracies resulting from the method of differencing, but to the inefficient distribution of the node points of the H-type grid in the area around the trailing edge. Support for this belief comes from the closeness of the two solutions over the rest of the airfoil, especially at the leading edge.

The poor resolution around the trailing edge is also believed to be the cause of the nonzero drag coefficient (a body traveling at subcritical speeds in an inviscid flow has zero drag). The pressure on the aft portion of the airfoil provides a forward thrust and, if it were underresolved, the drag calculated would be positive.

Figure 10 shows a comparison of the pressure distributions for the NACA 0012 airfoil with a Mach number of 0.8 and a 0 degree angle of attack. The curves virtually overlay each other, the main difference being at the shock. The triangle code appears to produce a sharper shock, but this is most likely due to the differences in node point distributions on the O- and H-type grid systems.

The 10 count difference in the drag coefficient is somewhat disturbing; however, in a comparison of results from the GAMM Workshop,[15] the drag coefficients calculated from fully conservative codes range from 0.0057 (Jameson) to 0.0070 (Holst). The discrepancy may again be attributed to the inadequate resolution of the aft thrust.

A sequence of pressure curves are plotted in Fig. 11. The parameters are the same as in Fig. 10 except that each curve represents a solution computed on a different mesh distribution. The range of the grid distributions is 16-128 points in the x (streamwise) direction and 4-32 points in the y (normal) direction. As the mesh size is decreased, the steady-state solutions approach a single solution. This is a numerical demonstration that the difference equations are convergent; that is, as the mesh decreases, the numerical solution converges to the solution of the differential equation.

Figure 12 is an accompanying graph showing the drag plotted against a characteristic mesh size squared (NX is the number of points in the x direction). A reasonable test for the accuracy of the difference equations is the convergence of the drag with decreasing mesh size. The straight-line fit implies that the equations are second-order accurate. This is suprising since the difference equations in supersonic flow are formally first-order accurate.

Figure 13 shows a plot of the convergence to the steady-state for the same transonic case as in Fig. 10. The convergence rate is computed from the formula

$$\text{Rate} = (\text{last residual}/\text{first residual})^{1/\text{No. iterations}}$$

and δ is a parameter that determines the position of the far-field boundary. The closer δ is to 1, the more stretched the mesh cells are in the far field.

Rapid convergence is obtained for the mesh with the lower-aspect-ratio cells. An iteration takes approximately 5 s of CPU time on a IBM 4341. Convergence is severely crippled, however, as the aspect ratio is increased. This is an undesirable

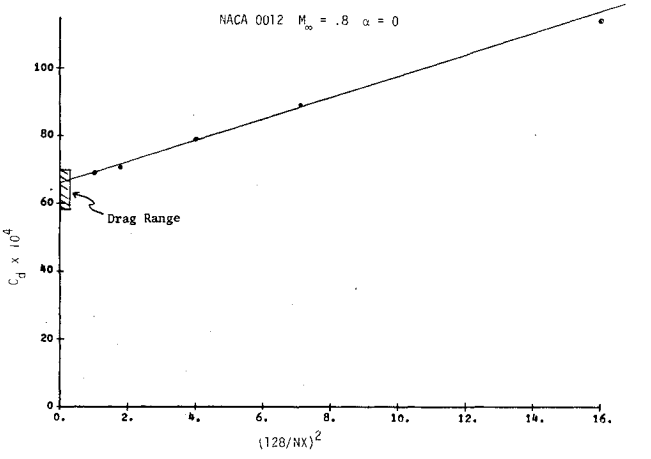

Fig. 12 Mesh refinement study: drag coefficient.

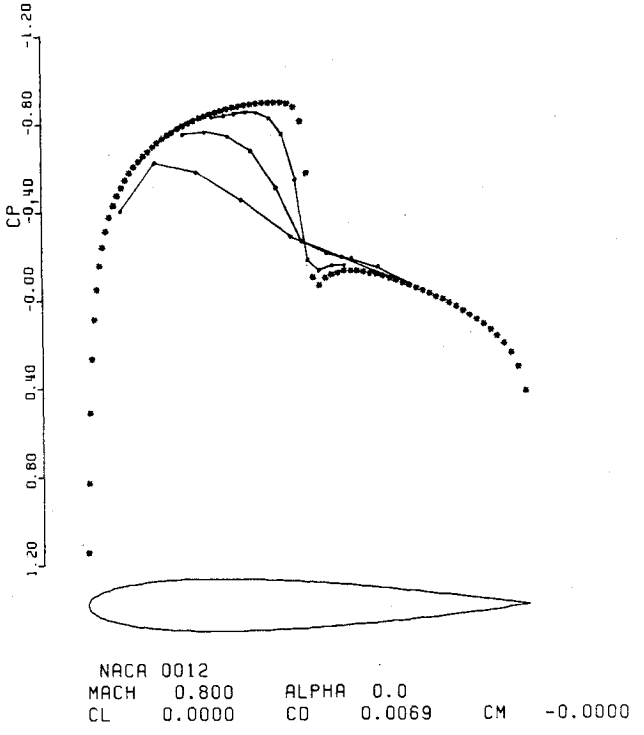

Fig. 11 Mesh refinement study: pressure distributions.

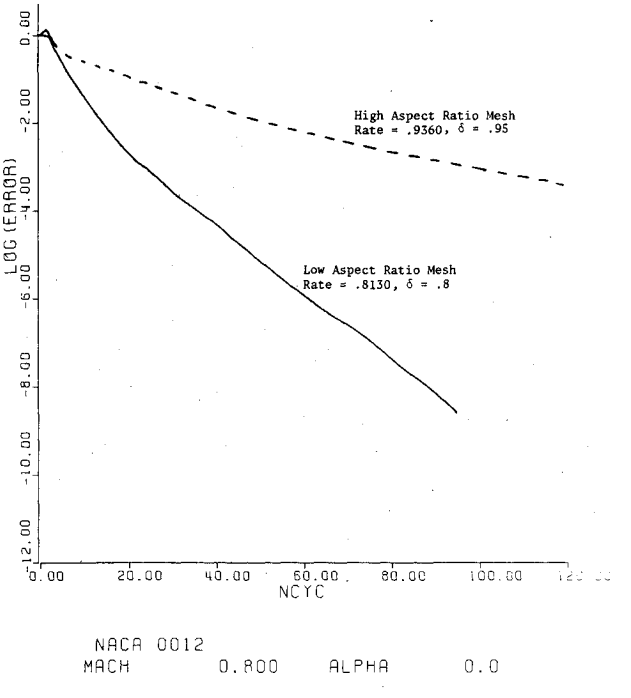

Fig. 13 Plot of convergence histories.

effect, since theoretically the boundary should be placed as far away from the airfoil as possible. The solution generated with the low-aspect-ratio cells has a slightly smaller supersonic zone due to blockage effects.

The fact that convergence is a function of the aspect ratio of the cells increases the attractiveness of unstructured grids having very low cell aspect ratios. Currently, implicit schemes that should take full advantage of the minimum-aspect-ratio property are being developed for unstructured grids.

The three-level, explicit scheme was used to obtain the present results for unstructured grids was very slow to converge.

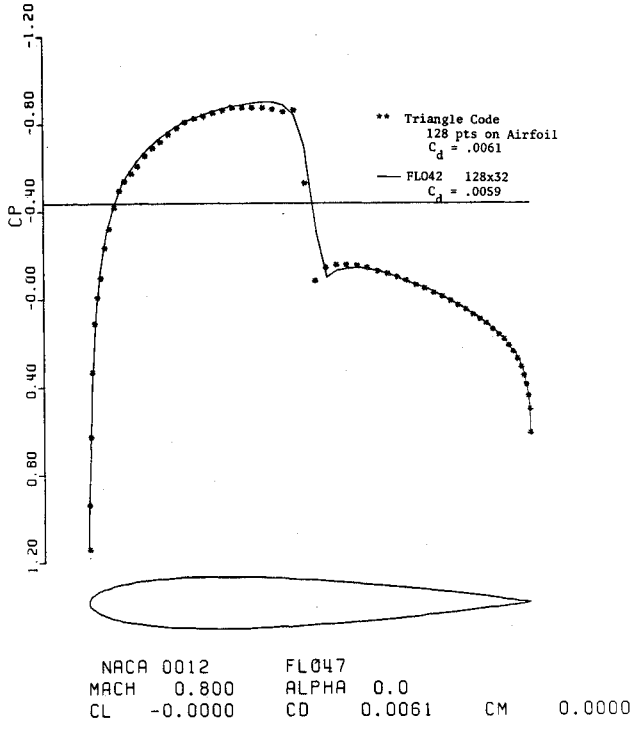

Fig. 14 Pressure distribution for supercritical case: unstructured grid.

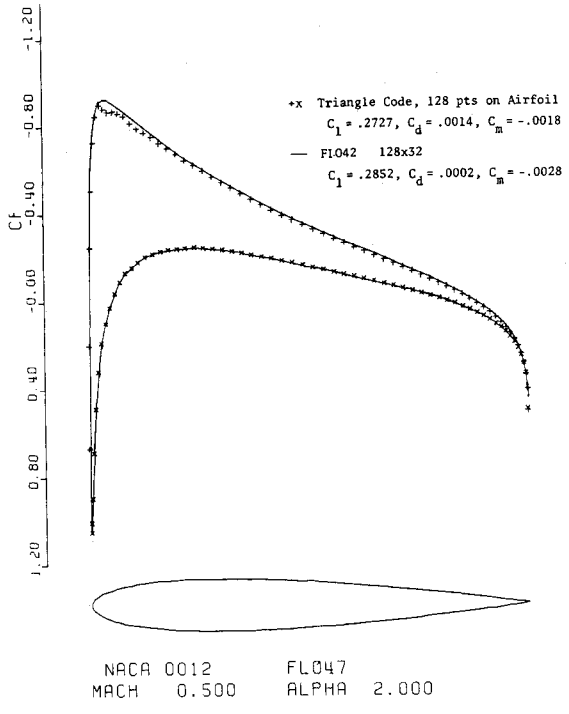

Fig. 15 Pressure distribution for lifting case: unstructured grid.

Thousands of iterations were required in order to achieve a steady-state solution with, say, four orders of magnitude reduction in the residual. This type of iteration speed is usual when using schemes with such compact support. However, this scheme can be easily vectorized since it is just a modification of the Jacobi scheme.

Figure 14 shows a comparison of the FLO42 code with a solution obtained on an unstructured grid. The pressure distributions compare well, except in the supersonic zone where there are slight oscillations. These oscillations are believed to be caused by the abrupt changes in the area and shape of the adjacent triangles along the airfoil surface; they are not believed to be caused by upwinding. Numerous smoothings of the artificial compressibility terms were tried with basically unchanged results.

Figure 15 shows a result obtained for a subcritical, lifting case. The triangle code does not resolve the suction pressure peak as well as FLO42. The oscillations at and around the peak can be also attributed to the same effect that caused the oscillations in the supersonic zone of the previous example. The Mach number at the peak is very close to 1. An incorrect resolution of the suction pressure would cause a somewhat higher drag to be calculated.

One way currently being explored to decrease the amplitude of the oscillations is smoothing the grid, i.e., moving some of the node points in such a way as to make the adjacent triangles more similar in area and shape. The center point of a hexagonal system of six triangles could be repositioned based on a criterion such as the area variation of each of the triangles from the mean being a minimum.

Conclusions

This paper contains the derivation of a triangular finite element method and a few examples demonstrating its accuracy, consistency, and convergence. The following conclusions can be made:

1) Difference equations can be easily constructed using the method outlined. The resultant equations can be viewed as forming a generalized flux balance for triangular elements and are experimentally determined to be second-order accurate.

2) To enforce the entropy condition, modifications of the difference equations by artificial compressibility can be made easily and efficiently.

3) Simple domains can be triangularized using conformal mapping techniques; however, the grid structure becomes difficult to maintain as the geometric complexity increases. The unstructured grid algorithms has the ability to triangularize complex domains.

4) With the multigrid-ADI iterative scheme, steady-state solutions can be arrived at within tens of iterations. While the explicit, three-stage scheme developed for unstructured grids is very slow, the computer time to reach the steady solutions can be speeded by vectorization of the code.

5) Solutions for test problems show close agreement with the FLO42 code. The triangular finite element scheme is less restrictive in grid geometry and is of comparable accuracy to the quadrilateral, finite volume code. The oscillations present in the pressure distribution show a sensitivity of the scheme to nonuniform mesh cells.

Clearly, the triangular finite element method is a viable alterative to more conventional methods that use quadilteral elements. The future of the triangular finite element method depends on whether one can successfully exploit the freedom that triangles have over other elements—that of handling more complex geometries.

References

[1]Farbridge, J.E. and Smith, R.C., "The Transonic Multi-Foil Augmentor-Wing," AIAA Paper 77-606, 1977.

[2]Habashi, W.G. and Hafez, M.M., "Finite Element Solution of Transonic Problems," AIAA Paper 81-147, 1981.

[3]Jameson, A. and Caughey, D.A., "A Finite Volume Method of Transonic Potential Flow Calculations," AIAA Paper 77-635, 1977.
[4]Thompson, J.F., "A Survey of Grid Generation Techniques in Computational Fluid Dynamics, AIAA Paper 83-447, 1983.
[5]Lapidus, L. and Pinder, G.F., *Numerical Solution of Partial Differential Equations in Science and Engineering,* John Wiley & Sons, New York, 1982.
[6]Bateman, H., "Notes on a Differential Equation Which Occurs in Two Dimensional Motion of a Compressible Fluid and the Associated Variational Problems," *Proceedings of the Royal Society of London,* Vol. 121, 1928, p. 194.
[7]Eberle, A., "Eine Method Finiter Elements Berechnungder Transsonicken PotentialStrimung un Profile," MMB, Berich Nr. UFE 1352 (0), 1977.
[8]Hafez, M., South, J., and Murman, E., "Artificial Compressibility for Numerical Solutions of Transonic Full Potential Equation," AIAA Paper 78-1149, 1978.
[9]Pelz, R.B. and Steinhoff, J.S., "Multigrid-ADI Solution of the Transonic Full Potential Equation for Airfoils Mapped to Slits," *Proceedings, ASME Winter Meeting,* Nov. 1981.
[10]Bank, R.E., "PLTMG User's Guide," Dept. of Mathematics, UCSD, Tech. Rept., June 1981.
[11]Jameson, A., "Acceleration of Transonic Potential Flow Calculations on Arbitrary Meshes by the Multiple Grid Method," AIAA Paper 79-1458, 1979.
[12]Brandt, A., "Multi-Level Adaptive Solution to Boundary Value Problems," *Mathematics of Computation,* Vol. 31, 1977, pp. 333-391.
[13]Peaceman, D.W. and Rathford, H.H., "The Numerical Solution of Parabolic and Elliptic Differential Equations," *SIAM Journal,* Vol. 3, 1955, pp. 28-41.
[14]Keller, J.D. and Jameson, A., "Preliminary Study of the Use of the STAR-100 Computer for Transonic Flow Calculations," NASA TM 74086, Nov. 1977.
[15]Rizzi, A. and Viviand, H., "Collective Comparison of the Solutions to the GAMM Workshop," *Numerical Methods for the Computation of Inviscid Transonic Flow with Shock Waves,* edited by Arthur Rizzi and Henri Viviand, Friedr. Vieweg and Sohn, Braunschweig/Wiesbaden, FRG, 1981, p. 167.